Materials Letters 186 (2017) 289–292

Contents lists available at ScienceDirect

Materials Letters

journal homepage: www.elsevier.com/locate/matlet

One-step synthesis of micro/nano flower-like $Ni_3V_2O_8$ as anode for Li-ion batteries

Yang Li[a], Ling-Bin Kong[a,b,*], Mao-Cheng Liu[a,b], Wei-Bin Zhang[a], Long Kang[a,b]

[a] State Key Laboratory of Advanced Processing and Recycling of Non-ferrous Metals, Lanzhou University of Technology, Lanzhou 730050, PR China
[b] School of Materials Science and Engineering, Lanzhou University of Technology, Lanzhou 730050, PR China

ARTICLE INFO

Keywords:
Microstructure
Nickel vanadate
Energy storage and conversion
Lithium ion batteries

ABSTRACT

A micro/nano flower-like $Ni_3V_2O_8$ superstructure composed of uniform two-dimensional (2D) nanoplates with thicknesses of 20–50 nm had been successfully synthesized using a facile one-step hydrothermal approach. It was found that the pH value of the mixed precursor solutions played a key role in the formation of flower-like $Ni_3V_2O_8$ structure. Importantly, the flower-like $Ni_3V_2O_8$ exhibited a high reversible capacity, good cycling stability (1047.8 mA h g^{-1} at 200 mA g^{-1} after 300 cycles), and superior rate capability (640.8 mA h g^{-1} at 3200 mA g^{-1}) as an anode material for Li-ion batteries. Furthermore, the lithium storage mechanism of $Ni_3V_2O_8$ involving in a conversion reaction and an intercalation reaction was proposed by *ex situ* XRD analyses.

1. Introduction

Nowadays, Li-ion batteries (LIBs) have attracted increasing attention for large-scale energy storage applications because of high energy density, long lifespan and environmental friendliness [1]. Although the graphite has been applied as commercial anode, it cannot meet the growing requirement for high energy/power storage devices due to its low specific capacity (372 mA h g^{-1}) [2]. Hence, much effort has been devoted to develop alternative electrode materials with desired electrochemical performances. Nickel oxide (NiO) has been well regarded as distinguished anode due to high capacity, low cost and worldwide abundance [3]. However, its practical application is largely restrained by poor cycle stability and large volume expansion during the charge/discharge process. One future avenue to solve the problems is to design various micro/nano electrode materials [4]. These secondary aggregated superstructures could not only enhance the effective interaction between the active materials and electrolyte, but also guarantee stable structure and favorable kinetics, particularly for the flower-like structures which showed satisfied electrochemical performance [5,6]. Recently, various mixed metal oxides have been explored to synergistically improve reversible capacity, electrochemical stability and rate capability of single-phase oxides via a suitable combination of different metal oxides [7]. Multiple vanadium oxides, as important mixed metal oxides, have received specific attention [8–14]. Only very recently, Wang et al. demonstrated $Ni_3V_2O_8$ exhibited promising anode application prospects in LIBs [15]. However, the synthesis route in that study required a complicated multi-step process, making the development of $Ni_3V_2O_8$ micro/nano structures time-consuming and costly. Therefore, it is of great significant to explore a facile, efficient and economical strategy to obtain micro/nano structured $Ni_3V_2O_8$ for improving its application.

In this work, we developed a simple one-step hydrothermal method to synthesize the micro/nano flower-like $Ni_3V_2O_8$, which showed a high specific capacity with an excellent cycling stability and rate capability as an anode material for LIBs. The possible lithiation-delithiation mechanism of $Ni_3V_2O_8$ was also discussed.

2. Experimental section

Dissolved 5.25 mmol of NH_4VO_3 into 80 mL deionized water at 80 °C with vigorous magnetic stirring, added 1.05 mmol $Ni(NO_3)_2 \cdot 6H_2O$ to the above solution under stirring, then adjusted pH value of the solution to about 9 using LiOH. After stirring for10 min, the obtained solutions were transferred into a 100 mL Teflon-lined autoclave, and maintained at 150 °C for 5 h. The resultant samples were then centrifuged, washed and dried overnight at 200 °C under vacuum. The micro/nano flower-like $Ni_3V_2O_8$ was obtained. For comparison, the bulk $Ni_3V_2O_8$ was obtained by controlling pH value of the mixed precursor solutions to about 7, while maintaining other reaction parameters unchanged. Details on synthesis, characterization and electrochemical measurements of as-prepared samples were described in the Supplementary Information (SI).

* Corresponding author at: State Key Laboratory of Advanced Processing and Recycling of Non-ferrous Metals, Lanzhou University of Technology, Lanzhou 730050, PR China.
E-mail address: konglb@lut.cn (L.-B. Kong).

http://dx.doi.org/10.1016/j.matlet.2016.10.018
Received 27 August 2016; Received in revised form 6 October 2016; Accepted 7 October 2016
Available online 08 October 2016
0167-577X/

3. Results and discussion

The XRD pattern of the flower-like $Ni_3V_2O_8$ presented in Fig. 1a indicated a clear $Ni_3V_2O_8$ phase (JCPDF card no. 74-1484) without any other crystalline phases. The SEM images showed the formation of a large number of micro/nano flower-like $Ni_3V_2O_8$ structures with an main diameter of about 1–4 μm (Fig. 1b). The micro/nano flowers were built from dozens of two-dimensional (2D) nanoplates with thicknesses of 20–50 nm (Fig. 1c and Fig. S1). Furthermore, the neighboring nanoplates were loosely interconnected with obvious open spaces existed between them (marked by red lines in Fig. 1c), which could accommodate the electrolyte, facilitating the intercalation/deintercalation of the Li-ion, thus enhance the performance of the electrode materials [16]. The TEM images agreed with those obtained from SEM as shown in Fig. 1d and e. The crystal lattice fringes were approximately 0.411 and 0.466 nm as shown by the HRTEM image (Fig. 1f), corresponding to the (200) and (120) planes of $Ni_3V_2O_8$, respectively. The selected area electron diffraction (SAED, the inset in Fig. 1f) pattern indicated that flower-like $Ni_3V_2O_8$ was polycrystalline. Both SEM and TEM images in Fig. S2 clearly demonstrated that the bulk $Ni_3V_2O_8$ with size of around several microns was obtained by controlling pH at about 7 in the mixed precursor solutions, while micro/nano flower-like $Ni_3V_2O_8$ was synthesized at pH 9. This indicated that the pH value of the mixed precursor solutions played a key role in the formation of flower-like $Ni_3V_2O_8$ superstructures.

Fig. 2a presented the initial three discharge-charge curves of the flower-like $Ni_3V_2O_8$. The initial discharge and charge capacities were 1596.8 and 1166 mA h g^{-1} with a Coulombic efficiency (CE) of 73%. The capacity loss was mainly due to irreversible phase transition and the formation of a solid electrolyte interphase (SEI) during the first cycle [9,12]. Furthermore, the flower-like $Ni_3V_2O_8$ displayed good cycling stability (Fig. 2b), and discharge capacity remained at 1047.8 mA h g^{-1} at 200 mA g^{-1} after 300 cycles, which was much higher than that of bulk $Ni_3V_2O_8$ (518.4 mA h g^{-1}). It clearly demonstrated that the micro/nano flower-like structure with sufficient void space between the neighboring nanoplates had the positive impacts on cycling stability. The flower-like structure can effectively promote the permeability of electrolyte, fully utilizing active materials, and accommodate the volume change of the $Ni_3V_2O_8$ during the cycling process. It was observed that the capacity of flower-like structure deteriorated slightly from 2nd to 100th cycle, and then increased gradually afterwards. Such capacity rise phenomena might be attributed to the reversible formation of a polymeric gel-like film came from the decomposition of electrolyte [17], and a possible activation process in the electrodes [18,19]. Furthermore, the CE increased distinctly from the first cycle to nearly 100% after 300 cycles, indicating the excellent cycling stability. Fig. 2c showed the electrochemical impedance spectroscopy (EIS) spectra of two samples after 3 cycles. In the equivalent circuit, R_s, R_{ct}, C_{dl} and Z_w were SEI film and/or contact resistance, charge transfer resistance, the double layer capacitance and Warburg impedance, respectively [12]. The R_{ct} of flower-like $Ni_3V_2O_8$ (30.8 Ω) was much smaller than that of bulk $Ni_3V_2O_8$ (61.2 Ω), suggesting higher electrical conductivity, and this was coherent with the charge-discharge results. Besides the high capacity and good cycling stability, the flower-like $Ni_3V_2O_8$ also showed an outstanding rate performance. As shown in Fig. 2d, even at a high rate of 3200 mA g^{-1}, a large capacity of 640.8 mA h g^{-1} was still reached. Upon altering the current density back to 100 mA g^{-1}, the capacity was recovered to 1179.9 mA h g^{-1}, demonstrating an outstanding rate and cycling performance. The thickness of nanoplates in the flower-like $Ni_3V_2O_8$ superstructures was thin enough, thus can shorten lithium transportation path and facilitate rate capability.

The cyclic voltammetric (CV) curves of flower-like $Ni_3V_2O_8$ (Fig. S3 in SI) were tested, and a series of ex-situ XRD patterns (Fig. 3) from the designated potentials (denoted with letters “a” to “f” in Fig. S3 and Fig. 3) had been obtained to understand the lithiation-delithiation behavior of $Ni_3V_2O_8$. When first discharging from the open circuit voltage to 1.66 V, the initial $Ni_3V_2O_8$ phase gradually turned to the NiO phase (JCPDF card no. 44-1159) and amorphous $Li_xV_2O_5$. During the subsequent discharging process, the new phase of Ni (JCPDF card no. 89-2387) appeared, which could be attributed to a conversion reaction of NiO to Ni companied with further insertion of Li^+ into the $Li_xV_2O_5$. During the subsequent charging process, Ni phases gradually disappeared and the NiO phase reappeared with the increase of charging degree, which corresponded to the extraction of Li^+ from $Li_xV_2O_5$ and the oxidation of Ni into NiO. Therefore, the lithium storage mechanism

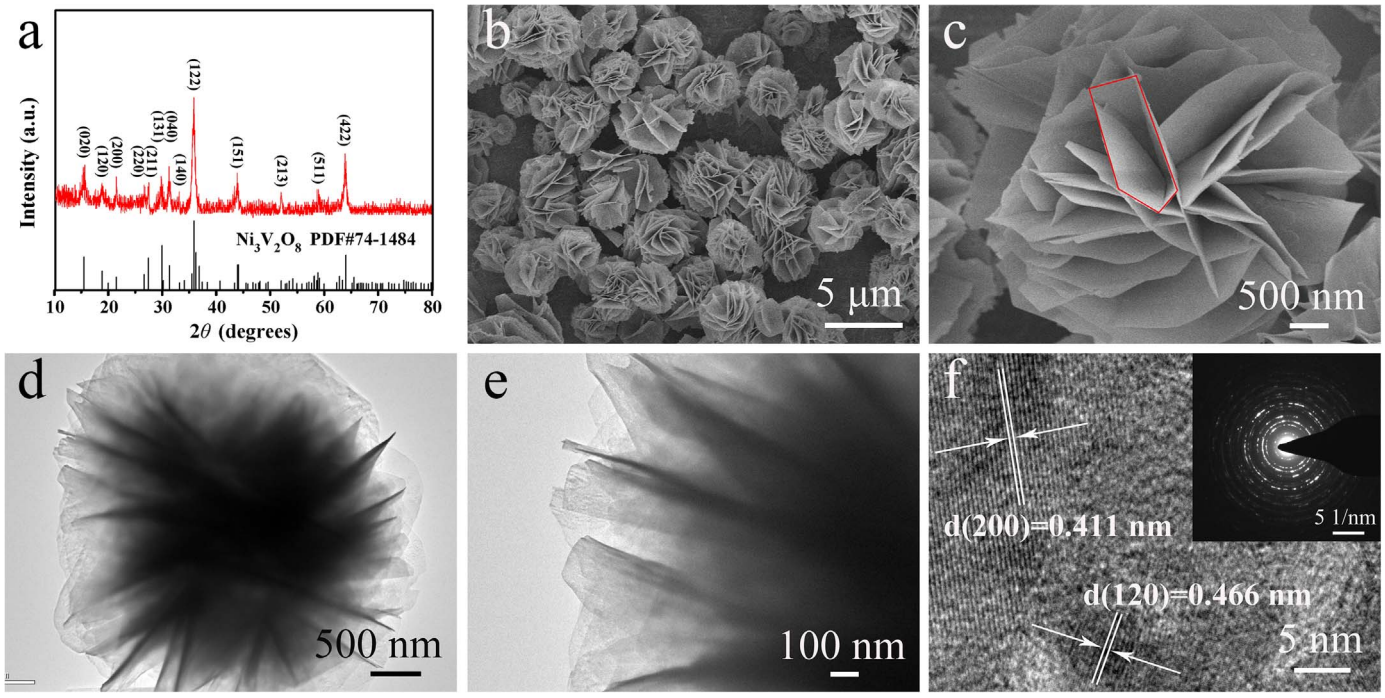

Fig. 1. (a) XRD patterns of flower-like $Ni_3V_2O_8$. (b, c) SEM and (d-f) TEM images of flower-like $Ni_3V_2O_8$ at different magnifications. The inset (f) was the SAED pattern of flower-like $Ni_3V_2O_8$.

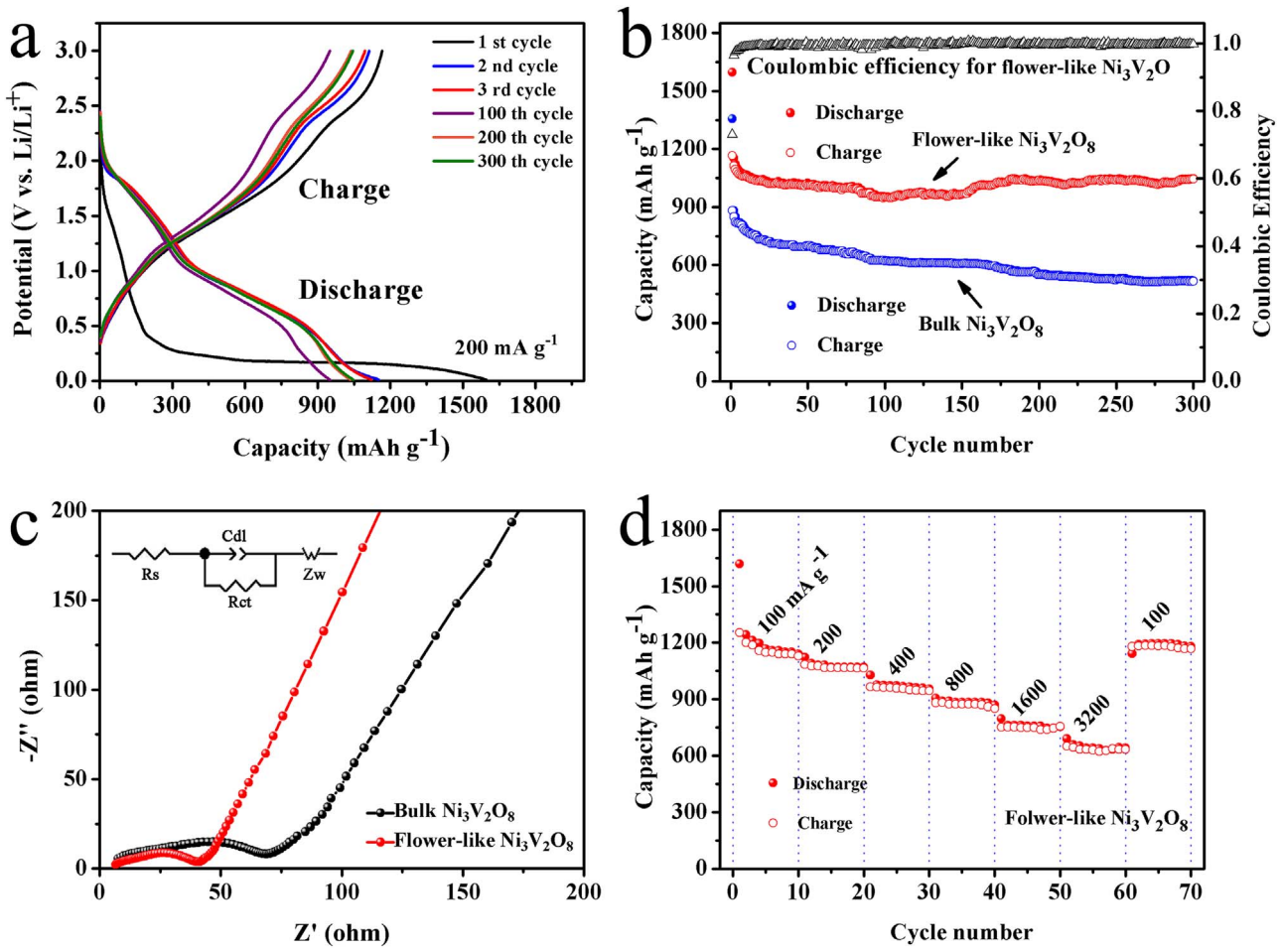

Fig. 2. (a) The charge/discharge curves of flower-like $Ni_3V_2O_8$. (b) The cycling performance and (c) EIS of the flower-like $Ni_3V_2O_8$ and bulk $Ni_3V_2O_8$. (d) The rate capabilities of flower-like $Ni_3V_2O_8$.

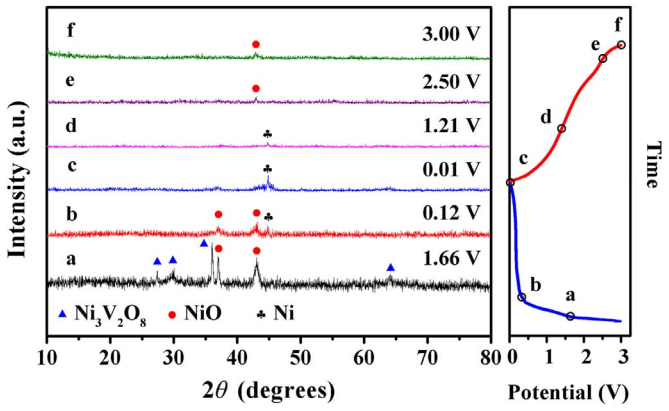

Fig. 3. The XRD patterns of flower-like $Ni_3V_2O_8$ under different discharge and charge states.

of $Ni_3V_2O_8$ involving in a conversion reaction and an intercalation reaction could be proposed based on above analyses.

4. Conclusions

We demonstrated, for the first time, a facile one-step hydrothermal method for the controlled synthesis of micro/nano flower-like $Ni_3V_2O_8$. The pH value of the mixed precursor solutions was found to play a crucial role in determining the final flower-like structure. With its unique micro/nano architecture and small sized nanoplate, the flower-like $Ni_3V_2O_8$ superstructure exhibited superior electrochemical performance as an anode material for LIBs. Furthermore, the electrochemical reaction process of $Ni_3V_2O_8$ with Li^+ was proposed, which indicated the common phenomenon in the conversion and intercalation reaction of metal vanadium oxide. The developed synthesis strategy might be readily generalized to construct other micro/nano structured multiple vanadium oxides. Moreover, this novel micro/nano flower-like $Ni_3V_2O_8$ superstructure might also be used in other fields including supercapacitor, sensor and water splitting photocatalyst.

Acknowledgments

The work was supported by the National Natural Science Foundation of China (no. 51362018) and the Foundation for Innovation Groups of Basic Research in Gansu Province (no. 1606RJIA322).

Appendix A. Supporting information

Supplementary data associated with this article can be found in the online version at doi:10.1016/j.matlet.2016.10.018.

References

[1] A. Manthiram, J. Phys. Chem. Lett. 2 (2011) 176–184.
[2] V. Aravindan, Y.S. Lee, S. Madhavi, Adv. Energy Mater. 5 (2015) 1402225.
[3] X. Sun, C. Yan, Y. Chen, W. Si, J. Deng, S. Oswald, L. Liu, O.G. Schmidt, Adv. Energy Mater. 4 (2014) 1300912.
[4] H.B. Wu, J.S. Chen, H.H. Hng, X.W. Lou, Nanoscale 4 (2012) 2526–2542.
[5] Y. Zhu, P. Nie, L. Shen, S. Dong, Q. Sheng, H. Li, H. Luo, X. Zhang, Nanoscale 7 (2015) 3309–3315.

[6] L. Li, Y. Cheah, Y. Ko, P. Teh, G. Wee, C. Wong, S. Peng, M. Srinivasan, J. Mater. Chem. A 1 (2013) 10935.
[7] C. Yuan, H.B. Wu, Y. Xie, X.W. Lou, Angew. Chem. Int. Ed. 53 (2014) 1488–1504.
[8] S. Denis, E. Baudrin, F. Orsini, G. Ouvrard, M. Touboul, J.M. Tarascon, J. Power Sources 81–82 (1999) 79–84.
[9] G. Yang, H. Cui, G. Yang, C. Wang, ACS Nano 8 (2014) 4474–4487.
[10] L.H. Gan, D. Deng, Y. Zhang, G. Li, X. Wang, L. Jiang, C.R. Wang, J. Mater. Chem. A 2 (2014) 2461.
[11] S. Ni, J. Ma, J. Zhang, X. Yang, L. Zhang, Chem. Commun. 51 (2015) 5880–5882.
[12] S. Ni, J. Ma, J. Zhang, X. Yang, L. Zhang, J. Power Sources 282 (2015) 65–69.
[13] J. Ma, S. Ni, J. Zhang, X. Yang, L. Zhang, Phys. Chem. Chem. Phys. 17 (2015) 21442–21447.
[14] S. Ni, X. Lv, J. Ma, X. Yang, L. Zhang, J. Power Sources 248 (2014) 122–129.
[15] C. Wang, D. Fang, H. Wang, Y. Cao, W. Xu, X. Liu, Z. Luo, G. Li, M. Jiang, C. Xiong, Sci. Rep. 6 (2016) 20826.
[16] Y.N. Ko, S.B. Park, K.Y. Jung, Y.C. Kang, Nano Lett. 13 (2013) 5462–5466.
[17] S. Grugeon, S. Laruelle, L. Dupont, J.M. Tarascon, Solid State Sci. 5 (2003) 895–904.
[18] S. Ni, X. Lv, J. Ma, X. Yang, L. Zhang, J. Power Sources 270 (2014) 564–568.
[19] S. Ni, X. Lv, T. Li, X. Yang, L. Zhang, Y. Ren, Electrochim. Acta 96 (2013) 253–260.